

Single-crystal synchrotron X-ray diffraction study of wüstite and magnesiowüstite at lower-mantle pressures

Steven D. Jacobsen, Jung-Fu Lin, Ross J. Angel, Guoyin Shen, Vitali B. Prakapenka, Przemyslaw Dera, Ho-kwang Mao and Russell J. Hemley

Copyright © International Union of Crystallography

Author(s) of this paper may load this reprint on their own web site provided that this cover page is retained. Republication of this article or its storage in electronic databases or the like is not permitted without prior permission in writing from the IUCr.

Single-crystal synchrotron X-ray diffraction study of wüstite and magnesiowüstite at lower-mantle pressures

Steven D. Jacobsen,^{a*} Jung-Fu Lin,^{a,b} Ross J. Angel,^c Guoyin Shen,^d Vitali B. Prakapenka,^d Przemyslaw Dera,^a Ho-kwang Mao^a and Russell J. Hemley^a

^aGeophysical Laboratory, Carnegie Institution of Washington, 5251 Broad Branch Road NW, Washington, DC 20015, USA, ^bLawrence Livermore National Laboratory, 7000 East Avenue, Livermore, CA 94550, USA, ^cDepartment of Geosciences, Virginia Polytechnic and State University, Blacksburg, VA 24061, USA, and ^dConsortium for Advanced Radiation Sources, University of Chicago, Chicago, IL 60637, USA. E-mail: s.jacobsen@gl.ciw.edu

This study demonstrates the use of monochromatic synchrotron X-ray radiation of 40 keV for high-precision equation-of-state studies on sets of single crystals analysed individually in the same diamond-anvil pressure cell. Angle-dispersive zone-axis diffraction patterns were obtained from crystals of wüstite-Fe_{0.93}O and magnesiowüstite-(Mg_{0.73}Fe_{0.27})O to 51 GPa in a hydrostatic helium pressure medium. The rhombohedral phase of Fe_{0.93}O was observed above 23 GPa, and its isothermal bulk modulus (K_0) was determined to be 134 (± 4) GPa, assuming $K' = 4$. The rhombohedral phase of Fe_{0.93}O is more compressible than B1-structured Fe_{0.93}O, with $K_0 = 146$ (± 2) GPa. Magnesiowüstite-(Mg_{0.73}Fe_{0.27})O remains cubic over the experimental pressure range, and has a bulk modulus of 154 (± 3) GPa with $K' = 4.0$ (± 0.1).

Keywords: single-crystal X-ray diffraction; megabar; zone-axis diffraction; diamond-anvil cell; wüstite; magnesiowüstite; helium pressure medium; equation of state.

1. Introduction

Thermodynamic equations of state have long played a central role in efforts to understand the nature of Earth's deep layered structure in terms of mineralogical (phase) and compositional variation (*e.g.* Duffy & Anderson, 1989; Ita & Stixrude, 1992; Jackson, 1998). Constraining the effects of pressure, temperature and composition on the structure and density of candidate high-pressure mineral assemblages is therefore one of the primary goals of mineral physics. Single-crystal compressibility studies have several distinct advantages over powder diffraction studies because the data are three-dimensional in nature, more data are available for least-squares fitting because symmetry-equivalent reflections are observed, and the diffraction peaks from a high-quality single crystal are nominally sharper than from a powder subject to intergranular stresses. Subtle phase transitions, such as lattice distortions, are readily observed in single-crystal diffraction data. Despite the advantages of using single-crystal samples for compressibility and structural studies, relatively few experiments on minerals have been carried out to pressures above ~ 20 GPa, mainly because working with fragile single-crystal plates at higher pressures requires careful attention to stress conditions of the sample, which can be minimized by the use of gas-loaded pressure media such as helium. Although

helium crystallizes at ~ 11 GPa (Besson & Pinceaux, 1979; Loubeyre *et al.*, 1993), solid helium remains sufficiently soft to be considered hydrostatic to pressures of at least 50 GPa (Takemura, 2001). Shu *et al.* (1998) reported the structure of single-crystal Fe_{0.95}O to 30 GPa in helium, Zha *et al.* (2000) measured the cell parameters of MgO to 55 GPa, also in helium and, most recently, Occelli *et al.* (2003) measured the equation of state of single-crystal diamond in helium to 140 GPa.

This study highlights the use of monochromatic synchrotron X-ray radiation at 40 keV for high-precision equation-of-state studies on sets of single-crystal samples loaded together in the same diamond cell in the 0.5 Mbar pressure range. X-ray beams of diameter 5–20 μm allow angle-dispersive X-ray diffraction patterns from different micro crystals to be recorded separately for ease of indexing. The use of very thin oriented plates (~ 10 μm thickness) and relatively high X-ray energies (~ 40 keV) results in zone-axis-type diffraction patterns from which high-precision cell parameters are obtained for equation-of-state fitting. Since the degree of oscillation necessary to obtain multiple classes of reflections is relatively small (typically $\pm 5^\circ$ ω), the standard centering procedures are adequate to keep the X-ray beam on a sample of similar dimensions as the beam. In this study, we present new data from two (of five) samples loaded simultaneously in

SXD at Mbar pressures

the same cell; wüstite- $\text{Fe}_{0.93}\text{O}$ and magnesiowüstite- $(\text{Mg}_{0.73}\text{Fe}_{0.27})\text{O}$. Whereas Fe_{1-x}O is more relevant to condensed matter physics as an archetypical transition metal oxide with strongly correlated electrons (e.g. Struzhkin *et al.*, 2001; Kantor *et al.*, 2004), $(\text{Mg,Fe})\text{O}$ is one of the most important minerals in Earth science because it is likely the most abundant non-silicate oxide in the planet, constituting roughly 10–20% by volume of the Earth's lower mantle. Our main objective here is to outline the single-crystal diffraction procedures and to report the high-pressure behaviour and equation-of-state parameters for wüstite and a magnesiowüstite crystal of relevant composition to the Earth's lower mantle.

2. Experiment

High-pressure single-crystal X-ray diffraction experiments were carried out on the BM-D beamline of GSECARS (sector 13) at the Advanced Photon Source. Monochromatic synchrotron X-rays were focused to a spot size $6\ \mu\text{m}$ wide by $20\ \mu\text{m}$ in height (FWHM) at 40 keV. The wavelength ($0.30996\ \text{\AA}$) was calibrated periodically using a CeO_2 standard. Diffraction images were recorded in transmission mode through the diamond cell on a MAR345 image plate positioned 38.58 cm from the sample.

Single-crystal $\text{Fe}_{0.93}\text{O}$ was synthesized by oxidizing a centimetre-sized single crystal of metallic iron at 1473 K and 10^{-11} atmospheres f_{O_2} in a CO/CO_2 gas-mixing furnace. The sample was drop-quenched into a container of the same CO/CO_2 mixture below the furnace to prevent the formation of magnetite upon cooling below $\sim 773\ \text{K}$. The recovered sample consisted of a coarse-grained aggregate of Fe_{1-x}O crystals, ranging in size from about 50 to $500\ \mu\text{m}$. The cell parameters of several Fe_{1-x}O crystals were measured to be in the range $4.298\text{--}4.300\ \text{\AA}$, corresponding to approximately $\text{Fe}_{0.93}\text{O}$ (McCammon & Liu, 1984). A single crystal of magnesiowüstite- $(\text{Mg,Fe})\text{O}$ containing $\sim 27\ \text{mol}\%$ FeO (sample Fe27) was synthesized by interdiffusing Fe and Mg between pre-reacted $(\text{Mg,Fe})\text{O}$ powders and single-crystal MgO . Details of the magnesiowüstite crystal synthesis are given elsewhere (Jacobsen *et al.*, 2002).

A crystal of $\text{Fe}_{0.93}\text{O}$ and $(\text{Mg}_{0.73}\text{Fe}_{0.27})\text{O}$, along with three other magnesiowüstite compositions and an annealed ruby-sphere pressure marker, were loaded together in a symmetric-type diamond-anvil cell (Fig. 1). Samples were pre-oriented on $\langle 110 \rangle$ in order to maximize the number of observable reflection classes, and polished into thin parallel plates using impregnated-diamond film to approximately $10\text{--}12\ \mu\text{m}$ thickness. The pressure cell was fitted with 50° full-cone WC seats and diamond anvils with $300\ \mu\text{m}$ flat culets. A rhenium gasket was pre-indented to 25 GPa ($\sim 35\ \mu\text{m}$ thickness) and the initial hole was drilled to $\sim 200\ \mu\text{m}$ diameter. The cell was loaded with compressed helium at $\sim 30\,000\ \text{psi}$, and initially compressed to $\sim 7\ \text{GPa}$. At this initial pressure, the gasket hole had reduced to $\sim 125\ \mu\text{m}$ diameter. At the highest pressure (51 GPa), the gasket hole had further reduced to $\sim 100\ \mu\text{m}$ diameter, and none of the $10\text{--}12\ \mu\text{m}$ -thick crystals

had bridged the gap between the diamonds based on visual observation and the diffraction patterns.

Zone-axis-type diffraction patterns were obtained from the pre-oriented thin-crystal platelets because the excitation error from Bragg diffraction is sufficiently low at 40 keV. At each crystal position the cell was oscillated about the vertical axis (ω) between $\pm 9^\circ$ for 60 s exposure times, resulting in the observation of two to three classes (six to 12 total reflections) for indexing and least-squares refinement (on d -spacings) using the *Unit Cell* refinement software package with regression diagnostics (Holland & Redfern, 1997). Unit-cell parameters were obtained at various pressures up to $\sim 51\ \text{GPa}$ using the ruby fluorescence pressure scale (Mao *et al.*, 1986). Hydrostatic conditions were maintained in the helium pressure medium to the maximum pressure, which was monitored by the separation of the R_1 and R_2 ruby fluorescence peaks, illustrated in Fig. 2. For the purpose of equation-of-state fitting, ambient-pressure cell parameters were determined outside the cell at 300 K.

3. Results and discussion

3.1. Wüstite- $\text{Fe}_{0.93}\text{O}$

In $\text{Fe}_{0.93}\text{O}$, six to ten reflections of the $h00$ and $hk0$ classes were available for indexing. A phase transition from the cubic ($B1$) structure to the rhombohedral (distorted- $B1$) phase was observed above 22 GPa upon splitting of the cubic 220 reflection into two sets of the rhombohedral 110 and 104 reflections, representing two (of the four) twin domains in the rhombohedral distortion (Shu *et al.*, 1998). Evolution of the 220 reflection with pressure is illustrated in Fig. 3, along with details (inset) from the image plate. We note that this is the highest pressure that the cubic phase of Fe_{1-x}O has been reported. Systematic errors in the pressure determination were ruled out as a cause for the discrepancy in the transition pressure compared with previous studies by checking zero-pressure ruby spectra outside the cell. The transition pressure of the rhombohedral distortion is known to depend on the stress conditions on and within the sample, and thus possibly

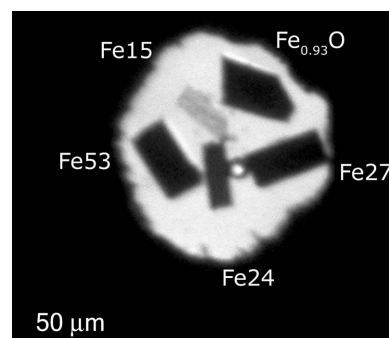


Figure 1

Five single-crystal samples of $(\text{Mg,Fe})\text{O}$ loaded into the same diamond cell for equation-of-state studies in the 0.5 Mbar range. Numbers indicate the percent of Fe in each sample. Here we report the behaviour of $\text{Fe}_{0.93}\text{O}$ and Fe27. The X-ray spot size on the samples was approximately $6\ \mu\text{m} \times 20\ \mu\text{m}$ (FWHM), allowing each crystal to be analysed individually. The gasket material is rhenium, and the culet size is $300\ \mu\text{m}$.

also on the degree of non-stoichiometry (x) of Fe_{1-x}O . In previous powder diffraction studies, the transition pressure typically ranges from about 8–10 GPa under non-hydrostatic conditions (Zou *et al.*, 1980; Dubrovinsky *et al.*, 2000; Fei & Mao, 1994) to roughly 16 GPa for both $\text{Fe}_{0.92}\text{O}$ and $\text{Fe}_{0.98}\text{O}$ under quasi-hydrostatic conditions (Yagi *et al.*, 1985; Fei & Mao, 1994). The transition pressure of $\text{Fe}_{0.95}\text{O}$ from the single-crystal study of Shu *et al.* (1998) in helium was 18 GPa.

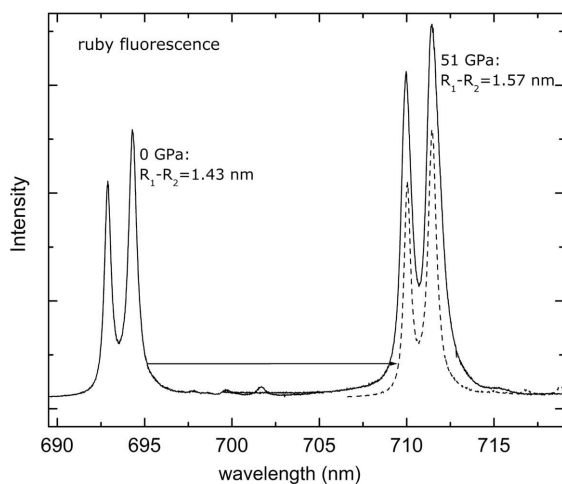


Figure 2 Ruby fluorescence spectra from outside the diamond cell at 1 atm (shorter wavelengths) and from 51 GPa (longer wavelengths). Hydrostatic pressure conditions were achieved in this experiment using a helium pressure medium. This figure illustrates minimal separation between the R_1 and R_2 fluorescence lines ($R_1 - R_2$ in nm), a proxy for differential stress in the cell. For comparison, the 1 atm spectrum is also shown shifted (dashed line) under the 51 GPa spectrum (solid line). The $R_1 - R_2$ separation at 50 GPa in a 4:1 methanol:ethanol pressure medium was reported to be 2.0 nm (Takemura, 2001).

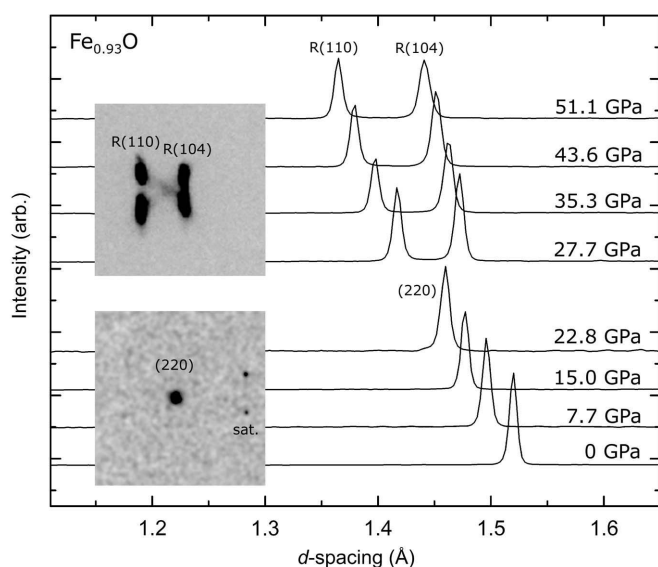


Figure 3 Evolution of the cubic 220 reflection in $\text{Fe}_{0.93}\text{O}$ to 51 GPa. The structure is still cubic at 22.8 GPa, as shown by the detail of the unsplit 220 peak with satellite reflections shown inset (origin is to the right). Splitting of the $R(110)$ and $R(104)$ reflections is completely resolved in the 27–50 GPa pressure range, and $\Delta d/d$ increases from 0.038 at 27 GPa to 0.054 at 51 GPa. There is no indication of additional splitting over this pressure range.

Although we could not observe the 111 reflection, previous studies indicate that splitting of the 220 and 111 reflections occurs simultaneously, so we conclude that the transition pressure in this study is elevated by 4–5 GPa compared with the previous single-crystal study (Shu *et al.*, 1998), further illustrating the enigmatic behaviour of Fe_{1-x}O at high pressure (Mao *et al.*, 1996).

The 200 reflections of the cubic phase are surrounded by a motif of satellite reflections at $(2 \pm \delta, 0, 0)$, $(2, \pm \delta, 0)$ and $(2 \pm \delta, \pm \delta, 0)$, connected along $h00$ by streaks of diffuse scattering (Fig. 4). The diffraction features around 200 are attributed to long-range order of defect clusters in the structure (Koch & Cohen, 1969; Gavarrri & Carel, 1989; Welberry & Christy, 1997). In agreement with previous X-ray studies at room pressure, we note that superlattice reflections are more intense on the low-angle side of the Bragg diffraction. Although the superlattice reflections decrease in intensity with increasing pressure as the rhombohedral phase is approached, they do not entirely disappear for the rhombohedral phase, and the $(2 \pm \delta, 0, 0)$ satellite on the low-angle side of 200 is especially apparent in the diffraction pattern of the rhombohedral phase at 28 GPa (Fig. 4c). The 200 Bragg reflection of the rhombohedral phase, *i.e.* $R(102)$, becomes broad along 020 (*i.e.* χ), but remains as sharp in 2θ as the cubic 200 at lower pressures.

Variation of the unit-cell parameters with pressure for the cubic and rhombohedrally distorted phases of $\text{Fe}_{0.93}\text{O}$ are given in Table 1. Volume–pressure curves are plotted in Fig. 5. We fitted the P – V data of cubic $\text{Fe}_{0.93}\text{O}$ to a third-order Birch–Murnaghan equation of state using the *EOS-FIT* (V5.2) least-

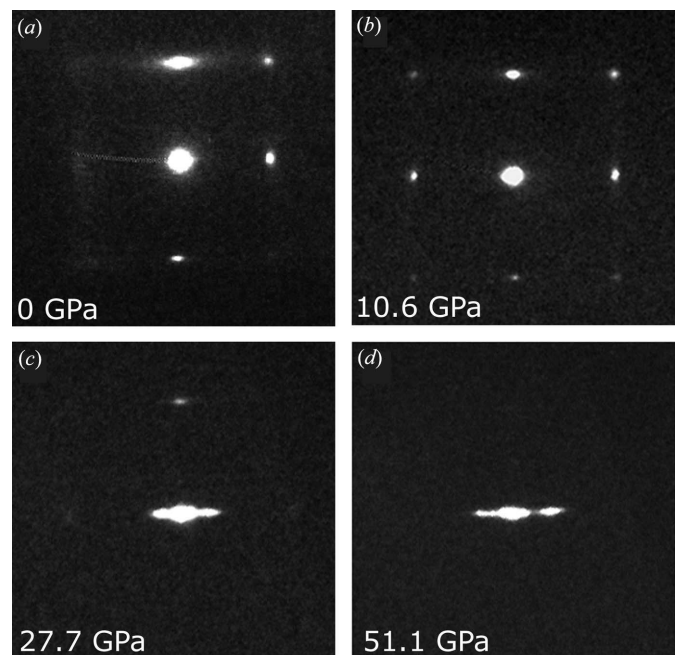


Figure 4 Evolution of the 200 reflection and surrounding superlattice reflections in $\text{Fe}_{0.93}\text{O}$ with pressure (the origin is vertical). The strongest satellite reflection at $(2 \pm \delta, 0, 0)$ is still observed in the rhombohedral phase, but is absent at pressures above ~ 40 GPa, indicating the disappearance of long-range order of defect clusters.

SXD at Mbar pressures

squares package (Angel, 2001). Since there are relatively few data points below 20 GPa, we fixed $K' = 4.0$ and varied V_0 and K_0 , resulting in $V_0 = 79.41 (\pm 0.04) \text{ \AA}^3$ and $K_0 = 146 (\pm 2) \text{ GPa}$, in good agreement with the bulk modulus for $\text{Fe}_{0.95}\text{O}$ of $149 (\pm 3) \text{ GPa}$ (Shu *et al.*, 1998) and for $\text{Fe}_{0.92}\text{O}$ of $147 (\pm 2) \text{ GPa}$ (Fei, 1996).

The measured molar volume data for the rhombohedral phase fall below the cubic-phase molar volumes calculated by extrapolating the equation of state of the cubic phase to pressures above the phase transition, as required by the thermodynamics of a phase transition that does not include a significant contribution from the entropy change accompanying the transition. We also note that the excess volume ($V_{\text{rhom}} - V_{\text{cubic}}$) arising from the transition does not extra-

polate to zero in the neighbourhood of the phase-transition pressure and, therefore, in contrast to previous studies (*e.g.* Shu *et al.*, 1998; Mao *et al.*, 1996), we propose that the transition is possibly weakly first-order in character.

Owing to the relatively low precision of previous powder diffraction studies [wherein the separation of $R(110)$ and $R(104)$ is not resolved] and limited pressure range of the previous single-crystal X-ray diffraction study (Shu *et al.*, 1998), the equation of state of the high-pressure rhombohedral phase of Fe_{1-x}O has not been previously determined. The distorted Fe_{1-x}O structure was predicted to be less compressible (higher bulk modulus) than cubic Fe_{1-x}O (Fei, 1996) based upon the variation of measured 200 d -spacings with pressure. We obtained unit-cell volumes of the rhombo-

hedral phase (set in the equivalent hexagonal cell, Table 1) to within a few parts in 10^4 , allowing us to estimate for the first time the compressibility of the high-pressure phase. We obtained an internally consistent equation of state by solving first for the parameters at a reference pressure of 28 GPa and then back-calculating zero-pressure parameters from the fit. Setting $P_{28\text{GPa}}$ as the reference pressure and fitting our experimental data between 28 and 51 GPa, we obtain equation-of-state parameters $V_{28\text{GPa}} = 51.28 (\pm 0.03) \text{ \AA}^3$ and $K_{28\text{GPa}} = 238 (\pm 4) \text{ GPa}$, with $K'_{28\text{GPa}} = 3.5$ (fixed). The fitted volume at 28 GPa is in excellent agreement with the experimental value of $51.27 (\pm 0.02) \text{ \AA}^3$ at 27.7 GPa. The rhombohedral phase equation-of-state parameters obtained by directly fitting the high-pressure data with a reference pressure of 28 GPa correspond to $V_0 = 59.85$, $K_0 = 132 \text{ GPa}$ and $K' = 4.2$. The P - V data were then fitted using an ambient reference pressure of 1 atm (but

Table 1
Unit-cell parameters for magnesiowüstite and wüstite at high pressure.

P (GPa)†	($\text{Mg}_{0.73}\text{Fe}_{0.27}\text{O}$)	Cubic $\text{Fe}_{0.93}\text{O}$	Rhombohedral $\text{Fe}_{0.93}\text{O}$		V (\AA^3)
	a (\AA)	a (\AA)	a (\AA)	c (\AA)	
0.00	4.2599 (3)	4.2980 (6)			
7.70	4.1953 (19)	4.2299 (13)			
10.6	4.1745 (7)	4.2085 (8)			
12.0	4.1660 (8)	4.1979 (22)			
13.7	4.1526 (28)	4.1842 (11)			
15.0	4.1440 (8)	4.1751 (23)			
22.8	4.0944 (15)	4.1255 (26)			
27.7	4.0707 (18)		2.8359 (7)	7.361 (4)	51.27 (2)
31.6	4.0514 (7)		2.8149 (8)	7.352 (4)	50.45 (3)
35.3	4.0332 (10)		2.7986 (14)	7.332 (7)	49.74 (4)
38.5	4.0172 (18)		2.7826 (10)	7.342 (5)	49.23 (3)
41.5	4.0037 (19)		2.7694 (9)	7.331 (4)	48.69 (3)
43.6	3.9941 (19)		2.7599 (20)	7.302 (10)	48.16 (6)
46.0	3.9865 (14)		2.7522 (11)	7.299 (5)	47.88 (3)
48.7	3.9747 (21)		2.7463 (30)	7.282 (15)	47.56 (9)
51.1	3.9641 (19)		2.7309 (18)	7.277 (9)	47.00 (5)

† Precision in the pressure determination is considered to be 0.05–0.1 GPa.

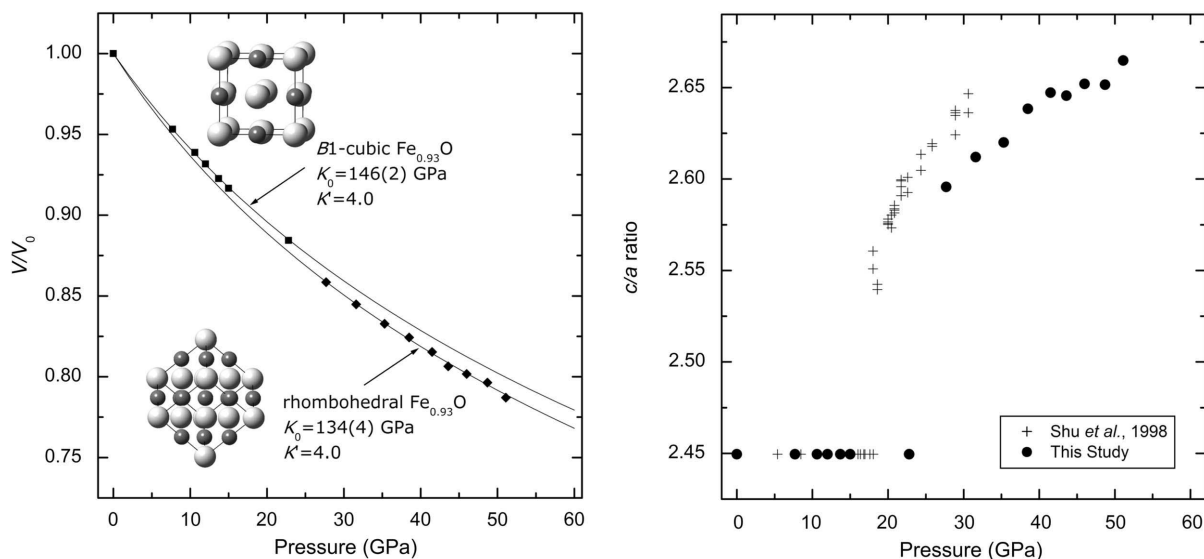


Figure 5

Left: normalized volume–pressure data for cubic and rhombohedral phases of $\text{Fe}_{0.93}\text{O}$ (filled symbols) with fitted equations of state (solid lines). Variation of the c/a ratio with pressure (filled circles) is shown on the right. The equation of state of the rhombohedral phase was determined first by fitting the high-pressure data to a 28 GPa reference pressure, and then back-calculating V_0 , K_0 and K' . Direct fitting of the P - V data (without a P_0 data point) yields consistent equation-of-state parameters (see text for details). Error bars are within the size of the symbols.

without the calculated V_0) using fixed $K' = 4.0$, resulting in $V_0 = 59.72 (\pm 0.22) \text{ \AA}^3$ and $K_0 = 134 (\pm 4) \text{ GPa}$, which are well within one standard deviation of the values obtained by extrapolating the $P_{28 \text{ GPa}}$ parameters back to P_0 . This cross-check demonstrates the internal consistency of the fitting method, and thus we conclude that a best estimate for the bulk modulus of rhombohedral $\text{Fe}_{0.93}\text{O}$ is $134 (\pm 4) \text{ GPa}$, assuming $K' = 4$. The higher compressibility (lower K_0) of the rhombohedral phase compared with the cubic phase is not thermodynamically inconsistent with a weakly first-order phase transition, nor is the fact that the calculated molar volumes at 1 atm are similar. We use the fitted V_0 of the rhombohedral phase (Table 1) to calculate $MV_0 = 11.99 (\pm 0.04) \text{ cm}^3$, corresponding to $\rho_0 = 5.667 (\pm 0.018) \text{ g cm}^{-3}$, which is within 2σ of the initial density of the cubic $\text{Fe}_{0.93}\text{O}$, with $MV_0 = 11.95 (\pm 0.001) \text{ cm}^3$ and $\rho_0 = 5.683 (\pm 0.003) \text{ g cm}^{-3}$.

It has also been proposed that Fe_{1-x}O adopts a lower-symmetry structure at higher pressures and 300 K, as evidenced by possible further splitting of the $R(104)$ peak above $\sim 40 \text{ GPa}$ (e.g. Yagi *et al.*, 1985; Fei, 1996). Additional splitting of $R(104)$ was not observed to 51 GPa in the current hydrostatic study, and there is no evidence for an additional transition in the evolution of the cla ratio with pressure (Fig. 5). Since the cubic-to-rhombohedral distortion was not evident in our single-crystal experiment until $P > 23 \text{ GPa}$ (compared with $\sim 16 \text{ GPa}$ in quasi-hydrostatic powder studies), it may also be expected that any subsequent (monoclinic) distortions would not occur until well above 40 GPa. The presence of an additional pressure-induced distortion is also suggested by the presence of a monoclinic ($C2/m$) phase of nearly stoichiometric $\text{Fe}_{0.99}\text{O}$ at 10 K, observed during a low-temperature neutron diffraction study (Fjellvåg *et al.*, 2002). Although we did not observe any further distortion of the rhombohedral phase to 51 GPa, the possibility that such a distortion was missed owing to the limited three-dimensional access to reciprocal space in the single-crystal diffraction experiment cannot be ruled out.

3.2. Magnesio-wüstite-($\text{Mg}_{0.73}\text{Fe}_{0.27}\text{O}$)

We also report the volume compression of a magnesio-wüstite crystal loaded in the same cell as the $\text{Fe}_{0.93}\text{O}$. Previous static-compression equation-of-state studies on magnesio-wüstite at 300 K and above 10 GPa have focused on either the MgO end member (e.g. Duffy *et al.*, 1995; Speziale *et al.*, 2001; Zha *et al.*, 2000; Fei, 1999) or on Fe-rich compositions containing 40 mol% FeO (Rosenhauer *et al.*, 1976), 60–80 mol% FeO (Richet *et al.*, 1989; Lin *et al.*, 2002) or between 80 and 95 mol% FeO (Mao *et al.*, 2002; Kondo *et al.*, 2004). Since lower-mantle compositions are expected to be somewhat lower (10–30 mol% FeO) (e.g. Andrault, 2001), we have undertaken a compressibility study of ($\text{Mg}_{0.73}\text{Fe}_{0.27}\text{O}$) because it is more applicable to the study of the Earth's interior.

In contrast to wüstite, the ($\text{Mg}_{0.73}\text{Fe}_{0.27}\text{O}$) sample does not exhibit a rhombohedral distortion over the experimental pressure range to 51 GPa. The absence of any phase transitions in this composition is consistent with previous shock-

wave data for ($\text{Mg}_{0.6}\text{Fe}_{0.4}\text{O}$) (Vassiliou & Ahrens, 1982) and from static compression of ($\text{Mg}_{0.6}\text{Fe}_{0.4}\text{O}$) to 26 GPa (Rosenhauer *et al.*, 1976). On the other hand, compositions containing greater than about 75 mol% Fe_{1-x}O do become rhombohedral above $\sim 20 \text{ GPa}$ (Mao *et al.*, 2002; Kondo *et al.*, 2004; Lin *et al.*, 2002), indicating that the addition of Mg to Fe_{1-x}O acts to stabilize the B1 structure at high pressure, consistent with recent single-crystal elasticity studies (Jacobsen *et al.*, 2004).

Volume–pressure data for ($\text{Mg}_{0.73}\text{Fe}_{0.27}\text{O}$) are listed in Table 1, and plotted in Fig. 6. The fitted equation-of-state parameters for this composition are $V_0 = 77.30 (\pm 0.09) \text{ \AA}^3$, $K_0 = 154 (\pm 3) \text{ GPa}$ and $K' = 4.0 (\pm 0.1)$. The bulk modulus obtained on a similar crystal (from the same bulk sample) with lower-pressure single-crystal data to $\sim 9 \text{ GPa}$ (Jacobsen *et al.*, 2002) is $158.4 (\pm 0.4) \text{ GPa}$ with $K' = 5.5 (1)$, somewhat higher than the current study. The difference in equation-of-state parameters between this study and those of Jacobsen *et al.* (2002) may be due to the limited pressure range of the previous study or from the use of different pressure scales (quartz volume *versus* ruby fluorescence). Our value of $K_0 = 154 (\pm 3) \text{ GPa}$ is also about 1σ below $K_0 = 157 (K' = 4)$ reported for (Mg,Fe)O containing $\sim 40 \text{ mol\% FeO}$ (Rosenhauer *et al.*, 1976), but it is in excellent agreement with the values of $K_0 = 154 (\pm 3)$ and $K' = 4.0 (\pm 0.4)$ recently reported for ($\text{Mg}_{0.64}\text{Fe}_{0.36}\text{O}$) (van Westrenen *et al.*, 2005). Equation-of-state parameters for (Mg,Fe)O are summarized in Table 2. The compression data for (Mg,Fe)O are plotted as the Birch-normalized pressure (F) against Eulerian strain (f) in Fig. 7, providing a more visual representation of how $K' = dK/dP \approx 4.0$. Despite these rather small differences in K for the iron-bearing magnesio-wüstites, we conclude that the bulk modulus of lower-mantle (Mg,Fe)O is not expected to vary from pure MgO by more than $\sim 10 \text{ GPa}$.

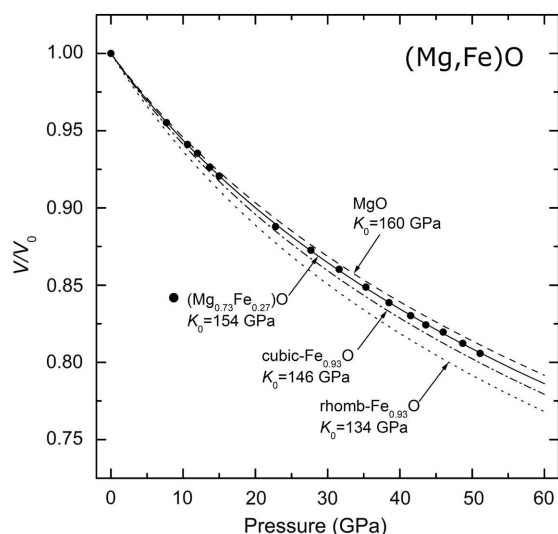


Figure 6

Comparative compressibility of single-crystal (Mg,Fe)O, with data from this study on ($\text{Mg}_{0.73}\text{Fe}_{0.27}\text{O}$) (solid line, filled circles, error within the symbol), cubic $\text{Fe}_{0.93}\text{O}$ (dash-dotted line) and rhombohedral $\text{Fe}_{0.93}\text{O}$ (dotted line). The equation of state of single-crystal MgO (Zha *et al.*, 2000) is shown by the dashed line.

SXD at Mbar pressures

Table 2

Equation-of-state parameters of (Mg,Fe)O from hydrostatic single-crystal compression studies.

	Cubic Fe _{0.95} O	Cubic Fe _{0.93} O	Rhomb Fe _{0.93} O	(Mg _{0.73} Fe _{0.27})O	MgO
<i>P</i> range (GPa)	0–18	0–51	23–51	0–51	0–55
ρ_0 (g cm ⁻³)	5.729	5.683 (±0.003)	5.667 (±0.018)	4.195 (±0.005)	3.585
<i>V</i> ₀ (Å ³)	79.88	79.41 (±0.04)	59.72 (±0.22)†	77.30 (±0.09)	74.68
<i>K</i> ₀ (GPa)	149 (±3)	146 (±2)	134 (±4)†	154 (±3)	160.2 (±0.7)
<i>K</i> '	4.0 (fixed)	4.0 (fixed)	4.0 (fixed)	4.0 (±0.1)	4.03 (±0.03)
Reference	Shu <i>et al.</i> (1998)	This study	This study	This study	Zha <i>et al.</i> (2000)

† Calculated by directly fitting the experimental *P*-*V* data with 1 atm reference pressure.

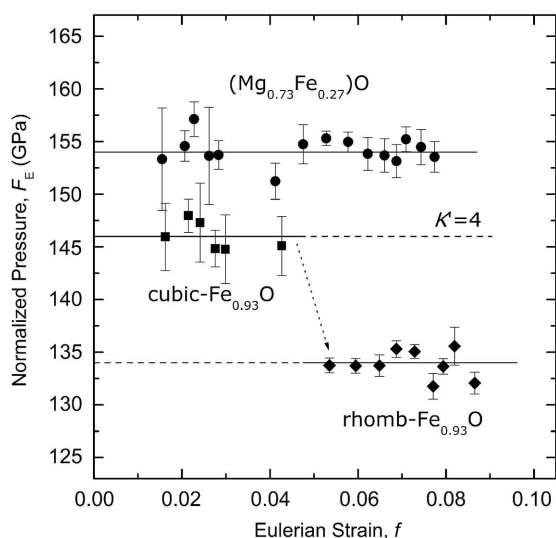


Figure 7

Plot of the Birch-normalized pressure (*F*) against Eulerian strain (*f*) for the Fe_{0.93}O and (Mg_{0.73}Fe_{0.27})O crystals. The plot visually confirms that *K*' is close to 4 for both Fe_{0.93}O phases. *K*' was allowed to refine in the (Mg,Fe)O data set, yielding 4.0 (±0.1). The values of *V*₀ used to calculate the *F*-*f* plot were determined experimentally for (Mg_{0.73}Fe_{0.27})O (*V*₀ = 77.30 ± 0.02 Å³) and cubic Fe_{0.93}O (*V*₀ = 79.40 ± 0.04 Å³), and were taken from the fitted equation of state for the rhombohedral phase of Fe_{0.93}O (*V*₀ = 59.72 ± 0.22 Å³).

4. Conclusions

Megabar equation-of-state studies on single-crystal mineral samples will soon be routine (Occelli *et al.*, 2003; Zha *et al.*, 2000; this study), and are expected to provide tighter constraints on the behaviour of minerals at very high pressure because cell parameters can be obtained to within a few parts in 10⁴ or better. The use of micro crystals measuring ~20 μm across and ~10 μm thick allows multiple compositions (or multiple orientations) to be loaded together in the same megabar cell, and the use of focused synchrotron X-rays at high energies (~40 keV) can be used to study the crystals individually at nominally identical pressures. In this study the equations of state of Fe_{0.93}O and (Mg_{0.73}Fe_{0.27})O were determined simultaneously. The quality of single-crystal diffraction patterns and the expanded pressure range over previous studies facilitated the determination of the equation of state of rhombohedrally distorted Fe_{0.93}O. In contrast to prediction, our results indicate that the rhombohedral phase of Fe_{0.93}O is more compressible than cubic Fe_{0.93}O.

We thank J. Shu for assistance with the helium gas loading, S. J. Mackwell for help with the (Mg,Fe)O sample synthesis, and C. T. Prewitt for discussions. Support for this study was provided by the National Science Foundation EAR-0440112 and a Carnegie Fellowship to SDJ, with additional support from the Carnegie/DOE Alliance Center. GSECARS is supported by the National Science Foundation – Earth Sciences (EAR-0217473), Department of Energy – Geosciences (DE-FG02-94ER14466) and the State of Illinois. Use of the APS was supported by the US Department of Energy, Basic Energy Sciences, Office of Energy Research, under Contract No. W-31-109-Eng-38.

References

- Andraut, D. (2001). *J. Geophys. Res.* **106**, 2079–2087.
 Angel, R. J. (2001). *Rev. Miner. Geochem.* **41**, 35–59.
 Besson, J. M. & Pinceaux, J. P. (1979). *Science*, **206**, 1073–1075.
 Dubrovinsky, L., Dubrovinskaia, N., Saxena, S. & LiBehan, T. (2000). *Mater. Sci. Eng.* **288**, 187–190.
 Duffy, T. S. & Anderson, D. L. (1989). *J. Geophys. Res.* **94**, 1895–1912.
 Duffy, T. S., Hemley, R. J. & Mao, H. K. (1995). *Phys. Rev. Lett.* **74**, 1371–1374.
 Fei, Y. (1996). *Mineral Spectroscopy: A Tribute to Roger G. Burns, Geochemical Society Special Publication No. 5*, pp. 243–254. St Louis, MO: The Geochemical Society.
 Fei, Y. (1999). *Am. Mineral.* **84**, 272–276.
 Fei, Y. & Mao, H. K. (1994). *Science*, **266**, 1678–1680.
 Fjellvåg, H., Hauback, B. C., Vogt, T. & Stølen, S. (2002). *Am. Mineral.* **87**, 347–349.
 Gavarri, J. R. & Carel, C. (1989). *Phase Trans.* **14**, 103–108.
 Holland, T. J. B. & Redfern, S. A. T. (1997). *Mineral. Mag.* **61**, 65–77.
 Ita, J. & Stixrude, L. (1992). *J. Geophys. Res.* **97**, 6849–6866.
 Jackson, I. (1998). *Geophys. J. Int.* **134**, 291–311.
 Jacobsen, S. D., Reichmann, H. J., Spetzler, H., Mackwell, S. J., Smyth, J. R., Angel, R. J. & McCammon, C. A. (2002). *J. Geophys. Res.* **107**, B2, 10.1029/2001JB000490.
 Jacobsen, S. D., Spetzler, H. A., Reichmann, H. J. & Smyth, J. R. (2004). *Proc. Nat. Acad. Sci. USA*, **101**, 5867–5871.
 Kantor, A. P., Jacobsen, S. D., Kantor, Y. K., Dubrovinsky, L. S., McCammon, C. A., Reichmann, H. J. & Goncharenko, I. N. (2004). *Phys. Rev. Lett.* **93**, 215502.
 Koch, F. & Cohen, J. B. (1969). *Acta Cryst.* **B25**, 275–287.
 Kondo, T., Ohtani, E., Hirao, N., Yagi, T. & Kikegawa, T. (2004). *Phys. Earth Planet. Inter.* **143/144**, 201–213.
 Lin, J. F., Heinz, D. L., Mao, H. K., Hemley, R. J., Devine, J. M., Li, J. & Shen, G. (2002). *Proc. Natl. Acad. Sci.* **100**, 4405–4408.
 Loubeyre, P., LeToullec, R., Pinceaux, J. P., Mao, H. K., Hu, J. & Hemley, R. J. (1993). *Phys. Rev. Lett.* **71**, 2272–2275.
 Mao, H.-k., Xu, J. & Bell, P. M. (1986). *J. Geophys. Res.* **91**, 4673–4676.

- Mao, H.-k., Shu, J., Fei, Y., Hu, J. & Hemley, R. J. (1996). *Phys. Earth Planet. Inter.* **96**, 135–145.
- Mao, W., Shu, J., Hu, J., Hemley, R. & Mao, H. K. (2002). *J. Phys. Condens. Matter*, **14**, 11349–11354.
- McCammon, C. A. & Liu, L. G. (1984). *Phys. Chem. Miner.* **10**, 106–113.
- Occelli, F., Loubeyre, P. & Letoullec, R. (2003). *Nature Mater.* **2**, 151–154.
- Richet, P., Mao, H. K. & Bell, P. M. (1989). *J. Geophys. Res.* **94**, 3037–3045.
- Rosenhauer, M., Mao, H. K. & Woermann, E. (1976). *Carnegie Inst. Wash. Yearb.* **75**, 513–515.
- Shu, J., Mao, H. K., Hu, J., Fei, Y. & Hemley, R. J. (1998). *N. Jahrb. Miner. Abh.* **172**, 309–323.
- Speziale, S., Zha, C. S., Duffy, T. S., Hemley, R. J. & Mao, H. K. (2001). *J. Geophys. Res.* **106**, 515–528.
- Struzhkin, V. V., Mao, H. K., Hu, J., Schwoerer-Böhning, M., Shu, J., Hemley, R. J., Strurhahn, W., Hu, M. Y., Alp, E. E., Eng, P. & Shen, G. (2001). *Phys. Rev. Lett.* **87**, 255501.
- Takemura, K. (2001). *J. Appl. Phys.* **89**, 662–668.
- Westrenen, W. van, Li, J., Fei, Y., Frank, M. R., Hellwig, H., Komabayashi, T., Mibe, K., Minarik, W. G., van Orman, J. A., Watson, H. C., Funakoshi, K. & Schmidt, M. W. (2005). *Phys. Earth Planet. Inter.* **151**, 163–176.
- Vassiliou, M. S. & Ahrens, T. J. (1982). *Geophys. Res. Lett.* **9**, 127–130.
- Welberry, T. R. & Christy, A. G. (1997). *Phys. Chem. Miner.* **24**, 24–38.
- Yagi, T., Suzuki, T. & Akimoto, S. (1985). *J. Geophys. Res.* **90**, 8784–8788.
- Zha, C. S., Mao, H. K. & Hemley, R. J. (2000). *Proc. Natl. Acad. Sci.* **97**, 13494–13499.
- Zou, G., Mao, H. K., Bell, P. M. & Virgo, D. (1980). *Carnegie Inst. Wash. Yearb.* **79**, 374–376.